Local topography and erosion rate control regolith thickness along a ridgeline in the Sierra Nevada, California

Emmanuel J. Gabet[1*], Simon M. Mudd[2], David T. Milodowski[2], Kyungsoo Yoo[3], Martin D. Hurst[4], and Anthony Dosseto[5]

[1] Department of Geology, San Jose State University, San Jose, California, USA
[2] School of GeoSciences, University of Edinburgh, Edinburgh, UK
[3] Department of Soil, Water, and Climate. University of Minnesota, St. Paul, Minnesota, USA
[4] British Geological Survey, Keyworth, Nottingham NG12 5GG, UK
[5] Wollongong Isotope Geochronology Laboratory, School of Earth and Environmental Sciences, University of Wollongong. Wollongong, NSW, Australia

* Correspondence to: Emmanuel Gabet, Dept. of Geology, San Jose State University, San Jose, California 95192. E-mail: manny.gabet@sjsu.edu

ABSTRACT: The ridgelines of mountain ranges are a source of geomorphic information unadulterated by the arrival of sediment from upslope. Studies along ridgecrests, therefore, can help identify and isolate the controls on important regolith properties such as thickness and texture. A 1.5-km section of ridgeline in the Sierra Nevada (CA) with a tenfold decrease in erosion rate (inferred from ridgetop convexity) provided an opportunity to conduct a high-resolution survey of regolith properties and investigate their controls. We found that regolith along the most quickly eroding section of the ridge was the rockiest and had the lowest clay concentrations. Furthermore, a general increase in regolith thickness with a slowing of erosion rate was accompanied by an increase in biomass, changes in vegetation community, broader ridgeline profiles, and an apparent increase in total available moisture. The greatest source of variation in regolith thickness at the 10–100-m scale, however, was the local topography along the

ridgeline, with the deepest regolith in the saddles and the thinnest on the knobs. Because regolith in the saddles had higher surface soil moisture than the knobs, we conclude that the hydrological conditions primarily driven by local topography (i.e., rapid vs. slow drainage and water-storage potential) provide the fundamental controls on regolith thickness through feedbacks incorporating physical weathering by the biota and chemical weathering. Moreover, because the ridgeline saddles are the uppermost extensions of 1st-order valleys, we propose that the fluvial network affects regolith properties in the furthest reaches of the watershed.

Introduction

The thickness of mobile regolith, defined here as material readily transported by biophysical processes (Yoo and Mudd, 2008; Mudd *et al.*, 2012; Anderson *et al.*, 2013) plays a critical role in numerous landscape processes. The regolith is the matrix for terrestrial life and its abundance at a particular location may modulate biological richness. For example, thick regolith is able to support a greater density of trees than thinner regolith because of its higher water-holding capacity (Meyer *et al.*, 2007). The regolith is also a reactor for chemical weathering processes (e.g., White *et al.*, 2002) and the longer average residence times of particles in a thicker mantle will yield an older and more weathered regolith (e.g., Mudd and Yoo, 2010). Furthermore, the thickness of regolith and its degree of weathering, as expressed by clay content, modulates its potential for landsliding in steep terrain (e.g., Selby, 1993). Finally, regolith thickness is

52 thought to be an important factor in controlling the weathering rates of underlying
53 bedrock (e.g., Heimsath *et al.*, 2001; Gabet and Mudd, 2010).
54 Studies have shown that, at the hillslope-scale, topographic curvature plays an
55 important role in the spatial distribution of regolith thickness and other fundamental
56 regolith properties (e.g., Hugget, 1975; Graham *et al.*, 1990), and this concept has been
57 formalized within predictive numerical models (Pelletier and Rasmussen, 2009; Tesfa *et*
58 *al.*, 2009). Convergent positions in the landscape, such as colluvial hollows, accumulate
59 material from adjacent slopes which, when added to regolith produced *in situ*, form
60 thick deposits (e.g., Reneau *et al.*, 1990). In contrast, divergent areas, such as hillslope
61 noses, are only supplied with regolith from local weathering processes and,
62 consequently, have a thinner mantle. However, it is difficult to isolate *in situ* controls of
63 regolith thickness on hillslopes because its depth at any point may be determined, in
64 large part, by colluvial inputs from upslope. In addition, whereas average regolith
65 depths across a catchment can be reasonably well predicted by accounting for
66 geomorphic processes at the broader scale (Pelletier and Rasmussen, 2009; Tesfa *et al.*,
67 2009), it is more difficult to predict the variability around that mean because of the
68 strong effect of local conditions (Phillips *et al.*, 2005; Nicotina *et al.*, 2011; Marshall and
69 Roering, 2014).
70 Ridgelines are sources of geomorphic information uncorrupted by sediment
71 delivery from upslope such that the properties of the regolith at any one spot are,
72 ideally, exclusively determined by the immediate environment (assuming a minimal
73 amount of dust deposition). Cascade Ridge, in the Feather River watershed in the

74 northern portion of the Sierra Nevada range of California, USA (Figure 1), is a
75 particularly advantageous site because a wave of incision through its bounding channels
76 has created a gradient in erosion rates along the ridge (Hurst *et al.*, 2013), thereby
77 offering an opportunity to evaluate the role of erosion rate, among other factors, in
78 controlling regolith properties. The character of the ridge, likely driven by the erosional
79 gradient, changes rapidly over a short distance (1.5 km), and we were thus able to
80 document changes in regolith properties at a relatively high spatial resolution. This
81 latter point is important because, as Gerrard (1990) has emphasized, high sampling
82 densities are critical where these properties are strongly determined by local conditions.
83 In addition, although the potential role of aeolian inputs at the site cannot yet be
84 dismissed, ongoing geochemical studies in the area (e.g., Yoo *et al.*, 2011) have not
85 found any notable elemental and mineralogical differences between the soil and the
86 bedrock and, therefore, do not support significant aeolian input of geochemically
87 distinct materials.
88 In addition to thickness, we measured a set of basic regolith properties that are
89 paramount to understanding pedogenic processes: texture, moisture, and organic
90 carbon concentration. The texture of regolith can yield information on its age and
91 weathering intensity (Birkeland, 1990). In addition, because water is a critical ingredient
92 in chemical weathering, consistent spatial variations in regolith moisture should drive
93 spatial differences in weathering depth and intensity (Pennock and de Jong, 1990).
94 Finally, the organic matter in regolith is important for water-holding capacity (Birkeland,
95 1999) and provides a first-order assessment of the input of carbon from the biota.

Field site

Cascade Ridge separates the Middle Fork Feather River (hereafter referred to as the Feather River) from one of its tributaries, Cascade Creek (Figure 1). The field area is underlain by Mesozoic plutonic rocks, primarily quartz diorite and tonalite (Saucedo and Wagner, 1992). In late Cretaceous-early Cenozoic times, the northern Sierra Nevada was at high altitudes, likely forming the western ramp of a high plateau (e.g., Cassel *et al.*, 2012 and references therein). As a result, deep valleys that traverse the range today, such as the canyons of the South Yuba River and the South Fork of the American River, had already been formed by the Eocene-Oligocene (e.g., Gabet, 2014 and references therein); although the antiquity of the Middle Fork Feather River canyon is not known, it is likely similar in age. Since this early period of uplift, the nothern Sierra Nevada has been tectonically quiescent (Cassel *et al.*, 2012; Gabet, 2014). Moreover, from the Eocene to the Miocene, this section of the range was buried and preserved by vast quantities of fluvial sediment and volcanic rocks. This material has been eroding away to re-expose the early Cenozoic landscape. Indeed, the remnants of these early-to-mid Cenozoic fluvial and volcanic sediment on upland surfaces and deep within valleys indicate that there has been little net topographic evolution of the northern Sierran landscape for much of the Cenozoic (Cassel *et al.*, 2012; Gabet, 2014). This long period of relatively slow erosion into basement rock, however, has been interrupted by recent incision of the Feather River and its tributaries in the vicinity of Cascade Ridge (Hurst *et al.*, 2012). Strath terraces along the trunk stream and the emergence of corestones from a thinning regolith along slopes bounding the Feather River attest to a significant

118 increase in erosion rate. Although the timing of the accelerated incision is unknown, we
119 suspect that it is related to the Ice Ages in the Sierra, a period when glaciers delivered
120 gravels and cobbles to the rivers and coarsened a bedload that was previously too fine
121 to efficiently abrade resistant bedrock (Gabet, 2014).
122 This recent incision along the Feather River has propagated into Cascade Creek
123 and up the hillslopes bracing Cascade Ridge. The lower end of the ridge, the one closer
124 to the junction between the Feather River and Cascade Creek, is at the crest of the
125 incision wave. Here, the ridge is sharp, narrow, rocky, bounded by steep slopes, and
126 vegetated with chaparral vegetation, such as manzanita (*Arctostaphylos spp*). As the
127 ridge reaches up into the older, low-relief part of the landscape, it becomes mantled
128 with regolith, it becomes progressively broader, and the aboveground biomass increases
129 (Milodowski *et al.*, 2015); concomitantly, the manzanita gives way to California black
130 oak (*Quercus kelloggii*) and canyon live oak (*Quercus chrysolepis*) trees. At the upper end
131 of the ridge, Douglas fir, sugar pine, and ponderosa pine dominate (*Pseudotsuga*
132 *menziesii*, *Pinus lambertiana*, and *Pinus ponderosa*, respectively). The climate in the area
133 is semi-arid, with 1750 mm of mean annual precipitation, and minimum/maximum
134 monthly temperatures typically ranging from -1/9 °C in the winter to 12/30 °C in the
135 summer (Daly *et al.*, 2008; PRISM, 2014). Soils along the ridge are rocky with an average
136 coarse fraction (>2 mm) of 50% (Soil Survey Staff, 2015). The soils lack B horizons or
137 have minimally developed B horizons which are yellowish, indicating that they are well
138 drained and in an early stage of chemical weathering. A horizon thicknesses are highly
139 variable but can be as thick as ~30 cm when determined solely based on color.

Depending primarily on the presence of B horizons, the soils are classified as either Sandy-skeletal, mixed, mesic Lithic Xerorthents (Waterman Series) or Coarse-loamy, mixed, superactive, mesic Typic Dystroxerepts (Chaix Series) (Soil Survey Staff, 2015).

Methods

Field measurements

The field study was carried out along a 1.5-km long section of Cascade Ridge; the transect begins in the rapidly eroding section of the ridge and, after gaining 200 m in elevation, ends in the slowly eroding section. The transect followed the visually-determined spine of the ridge as closely as possible although, in some instances, dense vegetation and steep rock outcrops forced lateral deviations of several meters. Measurements and soil samples were taken in late spring of 2011 and 2012, several weeks after the last significant rainstorms before the summer drought. Regolith thickness was measured with a tile probe (Mighty Probe^{TM}), a 135-cm shaft of reinforced steel with a T-handle and a sharpened tip. The probe was manually pushed into the regolith until refusal, and the depth of insertion was taken to be the thickness of the regolith. To validate the use of the instrument, measurements from the probe were compared to the boundary between the regolith and the undisturbed bedrock visually identified from four soil pits. Every 20 m along the transect, 10 regolith thickness measurements were taken with the tile probe at evenly spaced intervals within a 1 m^2 grid. If rock impeded the instrument at the regolith surface, we noted whether it was a clast or bedrock; if the former, its intermediate axis was measured. The

location of each measurement site was recorded with a GPS. At every other measurement site (i.e., every 40 m), a ~1-kg sample of the regolith surface, taken from the top 5 cm, was collected and stored in a sealed plastic bag. While awaiting analysis, the samples were kept in a refrigerator.

Laboratory analyses

The particle size distribution of the coarse fraction (> 63 μm) of each regolith sample was measured by sieving according to standard techniques (Burt, 2009). The particle size distribution of the fine fraction (≤ 63 μm) was determined with a Micromeretics (Norcross, GA) Sedigraph 5100 particle size analyzer. The regolith moisture content of each sample was determined as the percent difference between the original mass of a 10-15 g subsample and its mass after drying for 24 hours at 110° C (Burt, 2009). The amount of organic carbon in each sample was measured from a dried 5-10 g subsample of material passed through a 1-mm sieve to exclude plant litter. The subsamples were heated for 4 hours at 550° C in a muffle furnace and the loss on ignition (LOI) was determined as the percent difference between the original mass and the post-furnace mass (Burt, 2009).

Topographic analyses

Quantitative descriptions of the ridgeline topography along the transect are important for two reasons. First, knobs (local peaks) and saddles along the ridgeline create local environments important in regolith production. For example, the flow divergence from knobs is greater than from saddles and, thus, saddles should have

182 greater regolith moisture to drive chemical weathering processes. The 1-dimensional
183 (1D) topography along the crest was characterized by manually extracting the ridgeline
184 from a 1-m DEM (digital elevation model) created from LiDAR data (NCALM, 2008).
185 Because there is 200 m of relief along the ridge, the local topography was isolated from
186 the long-wavelength topography by fitting a 2^{nd} order polynomial to the ridgeline
187 elevation and subtracting the fitted elevation values from the actual elevations (Figure
188 2). To objectively identify saddles and knobs along the undulating topography of the
189 ridgecrest, the 1D topographic curvature at each point along the transect was calculated
190 by fitting a 2^{nd} order polynomial over successive sections of the ridge, delineated by a
191 sliding window advanced in 10-m increments, and taking its 2^{nd} derivative (Figure 3).
192 The window size, 320 m, was based on the average topographic wavelength along the
193 ridgeline (i.e., the average distance between the main saddles) (Figure 3B).
194 The ridgeline topography was also used to estimate erosion rates. In the same
195 area as the present study, Hurst et al. (2012) used ^{10}Be ages (n=21) to derive a
196 significant relationship between the 2-dimensional (2D) curvature of ridgetops and their
197 erosion rates. Following this approach, a 6-term polynomial function describing a 2D
198 surface was used to fit the digital topography within a 12-m x 12-m sliding window. This
199 window size corresponds to the scaling break that separates hillslope rugosity from
200 broader hillslope morphology (Roering *et al.*, 2010; Hurst *et al.*, 2012). The 2D curvature
201 at the midpoint of each window's position was determined as the 2^{nd} derivative of the
202 polynomial function. The erosion rate (E; m/y) was calculated from the 2D ridgeline
203 curvature (C_{2D}; 1/m) with

$$E = -\frac{\rho_s}{\rho_r} D C_{2D} \quad (1)$$

where ρ_s is the bulk density of the regolith (1300 kg/m^3), ρ_r is the density of rock (2600 kg/m^3), and D (0.0086 m^2/y) is the diffusion coefficient for soil creep processes (Hurst *et al.*, 2012).

Results

Erosion rates

The erosion rates calculated from the 2D ridgeline curvature (and converted to units of mm/y) range from 0.7 mm/y to 0.002 mm/y (Figure 4). The topography along the crest, however, has an important influence on the erosion rates calculated from the curvature. Because the 2D curvature of local peaks is relatively high, the knobs appear to be eroding more quickly than the saddles, thus obscuring the general trend in erosion rate along the ridgeline (Figure 4). To damp this topographic effect and capture large-scale differences in erosion rate, the calculated erosion rates were averaged over a 320-m sliding window (Figure 5); as before, the window size is the average topographic wavelength along the ridgeline. The smoothed erosion rate reveals three distinct erosional regimes along the transect: the end nearest the tributary junction is eroding at ~0.52 mm/y, the middle section at ~0.22 mm/y, and the end furthest from baselevel changes at ~0.06 mm/y. The rate calculated for the fastest-eroding section, however,

224 comes with an important caveat. Equation 1 assumes that the ridgeline has a cover of
225 mobile material diffused by creep processes; this end of the ridge, however, is rocky and
226 lacks a continuous regolith mantle. Moreover, 0.52 mm/y exceeds the range of
227 cosmogenically determined erosion rates used to calibrate Equation (1). For these
228 reasons, we cannot be certain that it is eroding at ~0.52 mm/y, only that it is eroding
229 more quickly than the rest of the ridge.

230 Regolith and Surface Properties

231 Rockiness

232 From the tile probe measurements, the *rockiness* (%) was calculated as the
233 frequency that the probe hit a large clast or bedrock at the surface within each 1-m^2 grid
234 (note, this is a different metric than the rock fragment estimates commonly given in soil
235 descriptions). A plot of the rockiness along the transect reveals two trends (Figure 6);
236 first, the lower portion of the transect where the landscape is eroding quickly is
237 substantially rockier than the rest of the ridgeline. Second, the rockiest portions of the
238 ridgeline are generally along the knobs and steep side-slopes. Where clasts were
239 present at the surface, their diameters ranged from 10 to 50 cm but there was no trend
240 in clast size along the ridge.

241 Regolith texture

242 The regolith texture classes of the surface samples along the ridge ranged from
243 sand to sandy loam but there was no clear spatial trend in this property. The clay-sized
244 particles (< 3.9 μm) changed significantly (t-test; $p < 0.001$) from one end of the transect

to the other. In the rapidly eroding section of the ridgeline (0 – 200 m), the clay concentration averaged 0.6 ± 0.5% (by weight relative to the bulk soil mass), whereas, along the rest of the transect, it averaged 2.2 ± 0.7%. Although the highest clay concentration was found in a saddle and the lowest on a knob, this soil surface property did not vary systematically with local topography. The coarse fraction concentration (> 2 mm) averaged 23 ± 12 % along the transect but did not appear to vary with either erosion rate or local topography. Recall, however, that we only sampled the soil surface along the ridgeline; in a more detailed study of particle sizes in this field area, Attal et al. (2014) found that hillslope soils coarsened with an increase in slope angle and erosion rate.

Regolith moisture

Although the regolith samples were taken from only the top 5 cm of the surface, their moisture content nevertheless showed a strong association with topographic position. Expressing the moisture of the surface samples as '%-dryness' (i.e., 100 - % moisture content) illustrates clearly the spatial correlation between the water content of the regolith and the local topography (Figure 7). The driest regolith was found on the knobs and the wettest was in the saddles.

Loss on ignition

The LOI of the <1 mm size fraction of the surface samples ranged from 5 – 25 % but did not change systematically along the ridgeline and, thus, did not appear to be influenced by erosion rate. Similarly, there was no clear effect of topography on LOI. The

absence of any relationships between LOI and topography or erosion rate may be due to short-term sediment transport events (e.g., faunalturbation) that introduce noise into underlying, long-term spatial trends. It is again important to note that the samples were taken from the surface of the regolith and likely do not reflect the total organic carbon in the regolith.

Regolith thickness

The penetration of the tile probe rarely came to a stop at a hard boundary, which would suggest the presence of a buried clast. Instead, the advance of the probe's tip was typically hindered by a transition to a gritty layer. At 4 sites along the ridge, the gritty refusal depth matched within 10 cm the regolith boundary visually identified from soil pits. Of the 750 thickness measurements, 72 were indeterminate because the regolith was deeper than the length of the tile probe (135 cm); the majority of these (78%) were in the slowly eroding portion of the ridge beyond the 1250-m mark. For the ensuing analyses, a value of 135 cm was assigned to these undetermined depths, thereby underestimating the true thicknesses.

The thicknesses reported here are the averages of the 10 measurements made within a 1-m^2 grid at each site. The average thicknesses were smoothed with a 100-m moving window to damp local variability (e.g., due to individual trees) and to resolve spatial trends more clearly at a scales relevant to the ridgeline geomorphic units (i.e., knobs, saddles, and side-slopes) (Figure 8A). Much of the variation in regolith thickness appears to be related to the local topography (Figure 8B). The deepest regolith is found in the saddles and the thinnest is on the knobs. However, partially obscured by the

topographic influence, the role of erosion rate can be detected as the regolith thickens toward the more slowly eroding portions of the ridgecrest. A comparison of the calculated erosion rate and regolith thickness suggests a linear relationship (albeit weak) between the two (Figure 9). The data also reveal that the range of regolith thickness increases with decreasing erosion rate; throughout the gradient in erosion rate, the minimum regolith thickness remains constant at ~10 cm while the maximum increases.

These analyses suggest that local topography and erosion rate exert the dominant controls on regolith thickness along Cascade Ridge. With the topography represented by the 1D ridgeline curvature (C_{1D}; m^{-1}), this hypothesis was tested with multiple regression analysis. Several equations of the form $H = f(C_{1D}, E)$ were explored, where H is regolith thickness (cm) and E is erosion rate (mm/y), including one in which an exponential form of E was assumed (i.e., $H = f(C_{1D}, e^{-aH})$ where a is a constant). The equation that yielded the best fit was a linear expression ($R^2 = 0.80$):

$$H(cm) = 10458C_{1D} - 155E + 81 \qquad (2)$$

where the erosion rate (mm/y) was determined with the 2D curvature (Equation 1) and smoothed over a 320-m sliding window (Figure 5). Recall that the regolith thickness at some sample sites in the slowly eroding portion of the transect was undetermined (i.e., deeper than 135 cm) and, thus, Eqn. (2) only represents a minimum regolith thickness at erosion rates < 0.1 mm/y.

It is important to note that, although the erosion rate was determined from the 2D curvature, this topographic metric is uncorrelated with the 1D curvature and, therefore, the predictor variables in Eqn. (2) are independent of each other (Figure 10). A comparison of the modeled and actual thicknesses smoothed with a 100-m sliding window indicates that the regression equation captures much of the variation in this property at the 100-m scale although, in the mid-range of thicknesses, there are errors as high as 25 cm (Figure 11). A regression of the predicted thicknesses against the raw (i.e., unsmoothed) thicknesses returned an R^2 of only 0.28, demonstrating that, at the meter-scale, variations in regolith depth are controlled by micro-site factors, such as the location of individual trees (e.g., Phillips and Marion, 2005; Phillips *et al.*, 2005; Roering *et al.*, 2010). In addition, the non-random distribution of regression residuals indicates that the topographic influence on regolith thickness is not fully captured by the 1D ridgeline curvature (Figure 12): regolith depths are consistently under-predicted on the knobs and over-predicted in the saddles. Different widths of the 1D curvature window were tried (from 6 – 400 m) but none resulted in better predictions. Finally, we emphasize that Equation (2) has not been tested elsewhere and may only be applicable at Cascade Ridge within the range of erosion rates determined along the transect.

Discussion

Regolith properties and ridgeline topography

To those familiar with mountainous terrain, it may not be surprising that the knobs along Cascade Ridge are rocky with thin regolith whereas the saddles have a

330 thicker mantle. Although it could be argued that the saddles host a deeper regolith
331 because of the accumulation of material from the bounding side-slopes, this does not
332 appear to be the case. The accumulation area (as determined with the ARCGIS D8
333 algorithm) for 61% of the sample sites along the spine of the ridge was either 0 or 1 m^2;
334 four drainage area values in the slowly eroding portion of the ridge, however, exceeded
335 30 m^2. Importantly, a linear regression of regolith thickness against accumulation area
336 returns an R^2 of 0.20 and, if the four values mentioned above are excluded, the R^2 falls
337 to 0.07. Thus, the assumption that regolith properties, including thickness, is dependent
338 on *in situ* conditions appears reasonable.
339 Of these conditions, the residence time of subsurface moisture may be the most
340 important in setting the spatial distribution of regolith thickness (Graham *et al.*, 1990).
341 Because of lower flow divergence and more topographic shading, the saddles retain
342 moisture for longer periods of time (Figure 7), thus driving higher rates of chemical
343 weathering compared to the knobs (e.g., Gabet *et al.*, 2006; Maher, 2010). A more
344 chemically weathered bedrock will be more hospitable to vegetation because it is
345 weaker, thereby allowing easier penetration by plant roots, and will have more pore
346 space to store water (Graham *et al.*, 2010). The plants, in turn, will accelerate physical
347 weathering of the bedrock (e.g., Phillips and Marion, 2005; Gabet and Mudd, 2010). The
348 additional moisture in the saddles, therefore, initiates a positive feedback loop between
349 deepening regolith and vegetation. The role of lithology at Cascade Ridge may be
350 particularly important because of the bimodal weathering behavior of plutonic rocks.
351 Unweathered plutonic rock is strong and resistant to physical weathering; however,

352 under a mantle of moist regolith, it becomes friable and weak because small fractures
353 allow fluid flow that leads to shattering by biotite hydration (Wahrhaftig, 1965;
354 Bazilevskaya *et al.*, 2013). The positive feedback between regolith weathering and
355 vegetation growth, as well as the bimodal weathering of plutonic rocks, may explain the
356 increasing range in regolith thickness as erosion rate slows (Figure 9). Indeed, as erosion
357 rate decreases along the ridge, topographic variations appear to play an increasingly
358 important role in the magnitude and spatial distribution of regolith thickness. Even
359 subtle changes in topography may lead to significant differences in regolith properties;
360 for example, spatial variations in erosion rate inferred from pedogenic hematite
361 (Sweeney *et al.*, 2012) may, instead, be due to differences in local hydrological
362 conditions (J. Roering, pers. comm.).
363 The role of topographic stresses in creating bedrock fractures (Miller and Dunne,
364 1996) may also contribute to the divergent evolutionary paths taken by the knobs and
365 saddles. The knobs in the more quickly eroding sections of the ridge were often
366 composed of large blocks separated by relatively wide (5 – 10 mm) fractures. Fractures
367 of this size, combined with the impermeable bedrock surface, would help to rapidly
368 drain precipitation from the knobs and create relatively dry conditions. The bedrock in
369 the saddles was covered by regolith and, thus, we cannot offer a comparison; however,
370 it is reasonable to postulate that bedrock underlying knobs and saddles would be
371 affected by different topographic stresses (Slim *et al.*, 2015).
372 Considering the potentially different physical and chemical weathering regimes
373 between knobs and saddles, we propose that the rate of regolith production along the

ridgeline is not solely dependent on regolith thickness (e.g., Heimsath *et al.*, 2001) but also on topographic position. The magnitude of the soil production function, typically represented as a plot of regolith production rate vs. regolith thickness, may vary along the ridgeline such that, for the same thickness of regolith, the production rate is greater in the saddles than on the knobs (Figure 13). A soil production function sensitive to topography implies that knobs and saddles could be eroding at the same rate, despite different regolith thicknesses.

Regolith properties and erosion rate

The topographic control on regolith thickness is imprinted over the general trend between thickness and erosion rate (Figure 9). Along the proximal section of the ridge, the erosion rate is too high to allow for the accumulation of a continuous mantle of regolith. In addition, the rate of regolith production is likely depressed by the sparseness of the vegetation (Figure 14) and the inability of the fractured bedrock surface to retain water. Consequently, the regolith there is thin, rocky, and limited to isolated patches. Moreover, the lower clay concentrations relative to the rest of the ridge attest to short residence times of weathered particles. As erosion rates slow beyond the 200-m mark on the ridgeline, the minimum regolith thickness remains approximately constant but the maximum regolith increases, leading to a greater average thickness.

Just as feedbacks between regolith development, regolith moisture, and vegetation appear to modulate the local topographic control on regolith thickness, similar relationships may also be important with respect to erosion rate. Hiking along

395 the Cascade Ridge transect in June 2012, we passed through a striking range of sensible
396 humidity in only 1.5 km: the ambient air at the faster-eroding end was quite dry while
397 the air at the slowly-eroding end felt substantially more humid. This steep gradient in
398 available moisture is reflected in the vegetation. The dry end is dominated by vegetation
399 adapted to arid conditions, such as manzanita (*Arctostaphylos*), while the wetter end is
400 vegetated by plants requiring more water, including patches of California corn lily
401 (*Veratrum californicum*), which is usually associated with meadows. In addition to a
402 difference in vegetation community along the transect, there is also a gradient in
403 aboveground biomass, with the slowly eroding section supporting about four times
404 more vegetation than the fastest eroding end (Figure 14); this pattern is consistent with
405 other observations across the region (Milodowski *et al.*, 2015). Given the short distance
406 (~1.5 km) and the 200 m change in elevation between the two ends of the transect, an
407 orographic effect on precipitation is likely not the source for the marked difference in
408 hydrological conditions along the ridge. We propose, instead, that the local hydrological
409 environment is ultimately controlled by the erosion rate and its effect on the ridgeline's
410 topography. Along the quickly eroding section, rapid drainage is encouraged by the
411 sharpness and narrowness of the ridge. Furthermore, the regolith is thin or absent and
412 precipitation runs quickly off the bedrock surfaces via widely spaced fractures. Bedrock
413 fractures at this location, therefore, may inhibit weathering by reducing the regolith-
414 water contact time (Twidale and Bourne, 1993; Gabet *et al.*, 2006) and slow the rate of
415 regolith production; this hypothesis contrasts with observations made elsewhere
416 (Phillips *et al.*, 2008; Marshall and Roering, 2014). The discrepancy may be due to

417 different topographic and climatic settings: one site was flat (Phillips *et al.*, 2008) and
418 the other was in a humid climate (Marshall and Roering, 2014). In both of these cases,
419 the near-surface environment can remain moist for long periods of time. However, the
420 steep slopes, thin regolith, and fractured rock along the rapidly eroding section of
421 Cascade Ridge dictate that, regardless of the absolute volume of precipitation, the
422 amount of moisture that can be stored is low and this is reflected in the drought-
423 tolerant vegetation and the relatively low biomass (Figure 14). Further up the transect
424 to the east, the slower erosion rates have formed a broader ridge mantled with thicker
425 regolith. Here, water infiltrates into the subsurface and gentle slopes prevent it from
426 draining quickly from the ridge. The higher regolith moisture favors chemical weathering
427 that creates porosity (Graham *et al.*, 2010) and weakens the bedrock to render it more
428 hospitable to biotic penetration. In addition, the higher regolith moisture combined with
429 the more weathered bedrock can support greater biomass which, in turn, deepens the
430 regolith even further through bioturbation. Positive feedbacks between topography,
431 hydrology, and vegetation can amplify small differences in the water balance to yield
432 large differences in regolith thickness (Goodfellow *et al.*, 2013).

433 Long-term evolution of Cascade Ridge

434 An interesting question is whether the corrugated topography of the ridgeline
435 can be maintained over long time-scales. Paradoxically, some evidence might suggest
436 that the knobs are eroding more quickly than the saddles. The peaks in local erosion
437 rate, calculated from the 2D curvature, generally correspond to the high points in the

438 local topography (Figure 4) – a geomorphologically reasonable conclusion since
439 sediment is transported from knobs over a wider range of directions than the saddles,
440 which are bounded on two sides by higher side-slopes. But if the knobs are eroding
441 more quickly, why are they there?

442 One possible explanation is that the difference in erosion rate between the
443 knobs and saddles is illusory. Recall that, according to Equation 1, the local erosion rate
444 was calculated as the product of the local 2D curvature and a diffusion coefficient
445 assumed to be constant along the entire length of the ridge. However, the diffusivity in
446 the saddles may be higher than on the knobs because of greater regolith thickness (e.g.,
447 Furbish, 2003; Pelletier *et al.*, 2011) and because greater moisture may stimulate
448 greater biotic activity which could drive faster rates of sediment transport (McGuire *et*
449 *al.*, 2014). In addition, the long-term average diffusivity may be effectively lower on the
450 knobs due to occasional supply-limited conditions. If, indeed, the diffusion coefficient
451 oscillates along the ridgeline, the saddles could be eroding as quickly as the knobs, and
452 the knob-and-saddle topography may be a steady-state condition. In addition, as noted
453 earlier, differences in regolith thickness between the knobs and saddles do not
454 necessarily imply that they are eroding at different rates if regolith production is
455 sensitive to topography.

456 Ultimately, the topographic wavelength of the ridge may be set by the spacing of
457 the tips of the channel network. Saddles along Cascade Ridge are typically the
458 uppermost extent of colluvial hollows hosting the heads of 1st order channels. Similarly,
459 the knobs are the terminal ends of spur ridges coming up from the valley bottoms

460 (Figure 15). Therefore, the ridgeline topography and its associated properties, such as
461 the spatial distribution of regolith, may be dictated by the reach of the fluvial network.
462 Because drainage density increases with erosion rate at this site (Hurst *et al.*, 2013), the
463 topographic wavelength along the ridgeline eventually may lengthen when the pulse of
464 incision has passed through the landscape and the channel network is pruned.

465 ## Conclusion

466 We exploited a 10-fold increase in erosion rate along a ridgeline in the Sierra
467 Nevada to explore the controls on regolith properties. We found that regolith thickness
468 generally decreases with erosion rate but that ridgeline topography (i.e., knobs and
469 saddles) plays a dominant role in controlling the variation in thickness. Indeed, the local
470 topography is so important that the subtle influence of erosion rate might not have
471 been recognized without the high-resolution sampling strategy that we adopted. The
472 thicker regolith in the saddles, attributed to longer water-residence times and a positive
473 feedback between water-holding potential and weathering, suggests that process-based
474 soil production functions should incorporate the role of subsurface hydrology. Finally,
475 because the saddles are the uppermost extent of 1^{st}-order valleys, we propose that the
476 variation in regolith thickness along Cascade Ridge may ultimately be controlled by the
477 tips of the fluvial network.
478
479 *Acknowledgements* - This work was supported by NSF-ARRA grant 0921440 to EG. The
480 participation of SM, KY, and MH was made possible by NSF-EAR grant 0819064. AD

481 acknowledges Australian Research Council Future Fellowship FT0990447 and Discovery
482 grant DP1093708. Thanks to A. Barkwith, J. Roering, and two anonymous reviewers for
483 helpful comments on the manuscript.

484

485 ## References

486 Anderson RS, Anderson SP, Tucker GE. 2013. Rock damage and regolith transport by
487 frost: an example of climate modulation of the geomorphology of the critical zone. Earth
488 Surface Processes and Landforms **38**: 299-316. DOI: 10.1002/esp.3330.

489 Attal M, Mudd SM, Hurst MD, Weinman B, Yoo K, Naylor M. 2014. Impact of change
490 in erosion rate and landscape steepness on hillslope and fluvial sediments grain size in the
491 Feather River Basin (Sierra Nevada, California). Earth Surface Dynamics **2**: 1047-1092.
492 DOI: 10.5194/esurfd-2-1047-2014.

493 Bazilevskaya E, Lebedeva M, Pavich M, Rother G, Parkinson DY, Cole D, Brantley SL.
494 2013. Where fast weathering creates thin regolith and slow weathering creates thick
495 regolith. Earth Surface Processes and Landforms **38**: 847-858.

496 Birkeland PW. 1990. Soil-geomorphic research - a selective review. Geomorphology **3**:
497 207-224.

498 Birkeland PW. 1999. Soils and Geomorphology. Oxford University Press: New York.

499 Burt R. 2009. Soil Survey Field and Laboratory Methods Manual. In *Soil Survey*
500 *Investigations Report No. 51*. Natural Resources Conservation Service, USDA: Lincoln,
501 Nebraska.

502 Cassel EJ, Graham SA, Chamberlain CP, Henry CD. 2012. Early Cenozoic topography,
503 morphology, and tectonics of the northern Sierra Nevada and western Basin and Range.
504 Geosphere **8**: 229-249.

505 Daly C, Halbleib M, Smith JI, Gibson WP, Doggett MK, Pasteris PP. 2008.
506 Physiographically sensitive mapping of climatological temperature and precipitation
507 across the conterminous United States. International Journal of Climatology **28**: 2031-
508 2064.

509 Furbish DJ. 2003. Using the dynamically coupled behavior of land-surface geometry and
510 soil thickness in developing and testing hillslope evolution models. In *Prediction in*
511 *Geomorphology*, Wilcock P, Iverson RM (eds). American Geophysical Union; 169-182.

512 Gabet EJ. 2014. Late Cenozoic uplift of the Sierra Nevada, California? A critical analysis
513 of the geomorphic evidence. American Journal of Science **314**: 1224-1257. DOI:
514 10.2475/08.2014.03.

515 Gabet EJ, Edelman R, Langner H. 2006. Hydrological controls on chemical weathering
516 rates at the soil-bedrock interface. Geology **34**: 1065-1068.

517 Gabet EJ, Mudd SM. 2010. Bedrock erosion by root fracture and tree throw: a coupled
518 bio-geomorphic model to explore the humped soil production function and the
519 persistence of hillslope soils. Journal of Geophysical Research **115**:
520 doi:10.1029/2009JF001526.

521 Gerrard AJ. 1990. Soil variations on hillslopes in humid temperate climates.
522 Geomorphology **3**: 225-244.

523 Goodfellow BW, Chadwick OA, Hilley GE. 2013. Depth and character of rock
524 weathering across a basaltic-hosted climosequence on Hawai'i. Earth Surface Processes
525 and Landforms. DOI: 10.1002/esp.3505.

526 Graham RC, Daniels RB, Buol SW. 1990. Soil-geomorphic relations on the Blue Ridge
527 front: I. regolith types and slope processes. Soil Science Society of America Journal **54**:
528 1362-1367.

529 Graham RC, Rossi AM, Hubbert KR. 2010. Rock to regolith conversion: producing
530 hospitable substrates for terrestrial ecosystems. GSA Today **20**: 4-9.

531 Heimsath AM, Dietrich WE, Nishiizumi K, Finkel RC. 2001. Stochastic processes of soil
532 production and transport: erosion rates, topographic variation and cosmogenic nuclides
533 in the Oregon Coast Range. Earth Surface Processes and Landforms **26**: 531-552.

534 Hugget RJ. 1975. Soil landscape systems: A model of soil genesis. Geoderma **13**: 1-22.

535 Hurst MD, Mudd SM, Walcott RC, Attal M, Yoo K. 2012. Using hilltop curvature to
536 derive the spatial distribution of erosion rates. Journal of Geophysical Research - Earth
537 Surface **115**: 1-19. DOI: 10.1029/2011JF002057.

538 Hurst MD, Mudd SM, Yoo K, Attal M, Walcott RC. 2013. Influence of lithology on
539 hillslope morphology and response to tectonic forcing in the northern Sierra Nevada of
540 California. Journal of Geophysical Research - Earth Surface **118**: 832-851. DOI:
541 10.1002/jgrf.20049.

542 Maher K. 2010. The dependence of chemical weathering rates on fluid residence time.
543 Earth and Planetary Science Letters **294**: 101-110.

544 Marshall JA, Roering JJ. 2014. Diagenetic variation in the Oregon Coast Range:
545 Implications for rock strength, soil production, hillslope form, and landscape evolution.
546 Journal of Geophysical Research: Earth Surface **119**: 1395-1417. DOI:
547 10.1002/2013JF003004.

548 McGuire LA, Pelletier JD, Roering JJ. 2014. Development of topographic asymmetry:
549 Insights from dated cinder cones in the western United States. Journal of Geophysical
550 Research: Earth Surface **119**: 1725-1750. DOI: 10.1002/2014JF003081.

551 Meyer M, North MP, Gray AN, Zald HSJ. 2007. Influence of soil thickness on stand
552 characteristics in a Sierra Nevada mixed-conifer forest. Plant Soil **294**: 113 - 123.

553 Miller DJ, Dunne T. 1996. Topographic perturbations of regional stresses and consequent
554 bedrock fracturing. Journal of Geophysical Research **101B**: 25,523-25,536.

555 Milodowski DT, Mudd SM, Mitchard ETA. 2014. Erosion rates as a potential bottom-up
556 control of forest structural characteristics in the Sierra Nevada Mountains. Ecology **in**
557 **press**. DOI: 10.1890/14-0649.1.

558 Milodowski DT, Mudd SM, Mitchard ETA. 2015. Erosion rates as a potential bottom-up
559 control of forest structural characteristics in the Sierra Nevada Mountains. Ecology **96**:
560 31-38. DOI: 10.1890/14-0649.1.

561 Mudd SM, Yoo K. 2010. Reservoir theory for studying the geochemical evolution of
562 soils. Journal of Geophysical Research: Earth Surface **115**. DOI: 10.1029/2009JF001591.

563 Mudd SM, Yoo K, Gabet EG. 2012. Influence of Chemical Weathering on Hillslope
564 Forms. In *Treatise on Geomorphology*, Shroder JF (ed). Academic Press: San Diego; 56-
565 65.

566 NCALM. 2008. Sierra Nevada, Oroville, CA. Mapping NCfAL (ed): Houston.

567 Nicotina L, Tarboton DG, Tesfa TK, Rinaldo A. 2011. Hydrologic controls on
568 equilibrium soil depths. Water Resources Research **47**. DOI: 10.1029/2010WR009538.

569 Pelletier JD, McGuire LA, Ash JL, Engelder TM, Hill LE, Leroy KW, Orem CA,
570 Rosenthal WS, Trees MA, Rasmussen C, Chorover J. 2011. Calibration and testing of
571 upland hillslope evolution models in a dated landscape: Banco Bonito, New Mexico.
572 Journal of Geophysical Research: Earth Surface **116**. DOI: 10.1029/2011JF001976.

573 Pelletier JD, Rasmussen C. 2009. Geomorphically based predictive mapping of soil
574 thickness in upland watersheds. Water Resources Research **45**. DOI:
575 10.1029/2008WR007319.

576 Pennock DJ, de Jong E. 1990. Regional and catenary variations in properties of Borolls
577 of southern Saskatchewan, Canada. Soil Science Society of America Journal **54**: 1697-
578 1701.

579 Phillips JD, Marion DA. 2005. Biomechanical effects of trees on soil and regolith:
580 Beyond treethrow. Annals of the Association of American Geographers **96**: 233-247.

581 Phillips JD, Marion DA, Luckow K, Adams KR. 2005. Nonequilibrium regolith thickness
582 in the Ouachita Mountains. Journal of Geology **113**: 325-340.

583 Phillips JD, Turkington AV, Marion DA. 2008. Weathering and vegetation effects in
584 early stages of soil formation. Catena **72**: 21-28.

585 PRISM. 2014. PRISM Climate Group. http://prism.oregonstate.edu.
586

587 Reneau S, Dietrich WE, Donahue DJ, Hull AJ, Rubin M. 1990. Late Quaternary history
588 of colluvial deposition and erosion in hollows, central California coast ranges. Geological
589 Society of America Bulletin **102**: 969-982.

590 Roering JJ, Marshall J, Booth AM, Mort M, Jin Q. 2010. Evidence for biotic controls on
591 topography and soil production. Earth and Planetary Science Letters **298**: 183-190.

592 Saucedo GJ, Wagner DL. 1992. Geologic map of the Chico quadrangle, California.
593 Division of Mines and Geology.

594 Selby MJ. 1993. Hillslope materials and processes. Oxford University Press: Oxford.

595 Slim M, Perron JT, Martel SJ, Singha K. 2015. Topographic stress and rock fracture: a
596 two-dimensional numerical model for arbitrary topography and preliminary comparison
597 with borehole observations. Earth Surface Processes and Landforms **40**: 512-529. DOI:
598 10.1002/esp.3646.

599 Staff SS. 2015. Official Soil Series Description.
600

601 Sweeney KE, Roering JJ, Almond P, Reckling T. 2012. How steady are steady-state
602 landscapes? Using visible–near-infrared soil spectroscopy to quantify erosional
603 variability. Geology **40**: 807-810.

Tesfa TK, Tarboton DG, Chandler D, McNamara J. 2009. Modeling soil depth from topographic and land cover attributes. Water Resources Research **45**. DOI: 10.1029/2008WR007474.

Twidale CR, Bourne JA. 1993. Fractures: a double edged sword. A note on fracture density and its importance. Zeitschrift fur Geomorphologie N.F. **37**: 495-475.

Wahrhaftig C. 1965. Stepped topography of the southern Sierra Nevada, California. Geological Society of America Bulletin **76**: 1165 - 1190.

White AF, Blum AE, Schulz MS, Huntington TG, Peters NE, Stonestrom DA. 2002. Chemical weathering of the Panola Granite: Solute and regolith elemental fluxes and the weathering rate of biotite. In *Water-Rock Interactions, Ore Deposits, and Environmental Geochemistry*, Hellman R, Wood SA (eds). The Geochemical Society; 37-59.

Yoo K, Mudd SM. 2008. Toward process-based modeling of geochemical soil formation across diverse landforms: A new mathematical framework. Geoderma **146**: 248-260.

Yoo K, Weinman B, Mudd SM, Hurst M, Attal M, Maher K. 2011. Evolution of hillslope soils: The geomorphic theater and the geochemical play. Applied Geochemistry **26**: S149-S153.

623 Figure captions

624

625 Figure 1. Site map. (Inset) Map of California with star indicating field site. (Main)
626 Hillshade of Cascade Ridge with transect delineated by the black line. The Middle Fork of
627 the Feather River is to the north of the ridge and Cascade Creek is to the south. The
628 Feather River, truncated by the left boundary of the image, flows from NE to SW and
629 forms a tributary junction with Cascade Creek (shown with the white star) and serves as
630 its baselevel. The 'A' and 'B' indicate the ends of the transect and are referred to in later
631 figures.

632

633 Figure 2. Second-order polynomial fit to ridgeline elevations along study reach. Ridgeline
634 elevations were subtracted from the polynomial to isolate the local topography. 'A' and
635 'B' refer to transect ends shown in Figure 1.

636

637 Figure 3. (A) Example of a ridgeline section fitted with a 2^{nd}-order polynomial over a
638 320-m sliding window. The topographic curvature at the midpoint of this section,
639 designated with the diamond, is the 2^{nd} derivative of the polynomial function, -0.0014.
640 (B) 1D curvature along ridgeline derived from 2^{nd}-order polynomial. Local topography
641 shown here to emphasize correspondence between curvature values and topography.
642 High positive curvatures are at the saddles and low negative curvatures are at the
643 knobs.

644

645 Figure 4. Erosion rate calculated from 2D curvature compared to the local ridgeline
646 topography. The erosion rate calculation appears to be influenced by the local
647 topography whereby the knobs have higher erosion rates than the saddles.
648
649 Figure 5. Erosion rate calculated from 2D ridgeline curvature averaged over a 320-m
650 window to reduce the effects of the local topography. There appear to be 3 different
651 erosional regimes along the transect: ~0.52 mm/y along the proximal portion, ~0.22
652 mm/y in the middle, and ~0.06 mm/y along the distal section. The transition between
653 each section is not sharp, likely a consequence of a gradual geomorphic adjustment to
654 the advance of the incision wave(s).
655
656 Figure 6. Comparison of surface material and local topography. The rapidly eroding end
657 of the transect (0 – 200 m) has a substantially greater amount of large clasts and
658 bedrock at the surface than the slowly eroding portions. Knobs and steep sideslopes
659 tend to be more rocky although the relationship between rockiness and topography is
660 not strong.
661
662 Figure 7. Soil dryness (i.e., 100 - % moisture) and local topography along the ridge. The
663 driest regolith is associated with knobs and southwest-facing sideslopes. Wettest
664 regoliths in the saddles. Dashed line fit by eye to emphasize trends in regolith moisture.
665 Regolith moisture represented by 'dryness' to facilitate comparison with the local
666 topography.

667

668 Figure 8. (A) Regolith thickness along the transect. A 5-pt moving average of thickness
669 reveals a sinusoidal pattern along the ridge. (B) Regolith thickness (moving average) and
670 local topography are nearly mirror images of each other. The regolith is thickest in the
671 saddles and thinnest on the knobs. Note the general increase in regolith thickness
672 towards the distal end of the transect where the erosion rates are lower.

673

674 Figure 9. Regolith thickness vs. calculated erosion rate. The erosion rate used here is the
675 smoothed rate shown in Figure 5. Because regolith thickness exceeded the reach of the
676 probe in the slowly eroding portion of the ridge, the data points in the upper left of the
677 plot under-represent the true thickness and, as a result, the slope of the regression
678 should be steeper. Although the data might also be fit with a negative logarithmic
679 function (i.e., the steady-state solution to an exponential soil production function),
680 granite weathering is best described by a humped soil production function (SPF)
681 (Wahrhaftig, 1965). Furthermore, invoking a single SPF for all topographic positions
682 along the ridgeline is likely not appropriate. Given these complications, a linear fit to the
683 data is the most conservative approach.

684

685 Figure 10. Plot of 2D curvature and erosion rate vs. 1D ridgeline curvature. Although the
686 erosion rate was calculated from the 2D curvature, it is uncorrelated with the 1D
687 curvature. The spatial autocorrelation in the raw data is due to the sliding-window
688 technique of calculating the 1D curvature. The 'smoothed erosion rate' was determined

689 by averaging over a 320-m sliding window to damp the effects of local topography on
690 the calculation of erosion rate (see Figure 5). The three erosional regimes create the
691 three plateaus seen in the line plot.
692
693 Figure 11. Regolith thickness modeled from the 1D ridgeline curvature and the
694 calculated erosion rate. Measured regolith thickness values were smoothed with a 5-pt
695 moving window to damp meter-scale variations not captured in our study. The similarity
696 between the modeled and actual regolith thicknesses suggest that 1D curvature and
697 erosion rate are the primary factors in controlling regolith thickness along Cascade Ridge
698 at the 10^2-m scale. The constant in the regression indicates that regolith thickness is
699 consistently underpredicted, albeit by a small amount.
700
701 Figure 12. Residuals from the regolith thickness regression equation compared to the
702 local topography. The non-random distribution of the residuals indicates that the 1D
703 ridgeline curvature is not fully capturing the effects of the local topography.
704
705 Figure 13. Different soil production functions depending on topographic position.
706 Although knobs and saddles may be eroding at the same rate, they may host different
707 steady-state regolith thicknesses because of different local conditions (indicated by
708 stars). For example, saddles may have higher rates of regolith production for a given
709 regolith thickness because they remain wetter for longer periods of time.
710

711 Figure 14. Aboveground biomass and local topography along the ridge. Biomass
712 increases nearly 4-fold from the rapidly eroding portion of the ridge to the slowly
713 eroding portion. Biomass determined with mean canopy heights derived from LiDAR
714 data (Milodowski *et al.*, 2014).
715
716 Figure 15: Knobs (stars) and basins along Cascade Ridge. The knobs along Cascade Ridge
717 are often the uppermost extent of spur ridges bounding the basins that drain from the
718 ridge to the valley bottom (shaded).
719
720

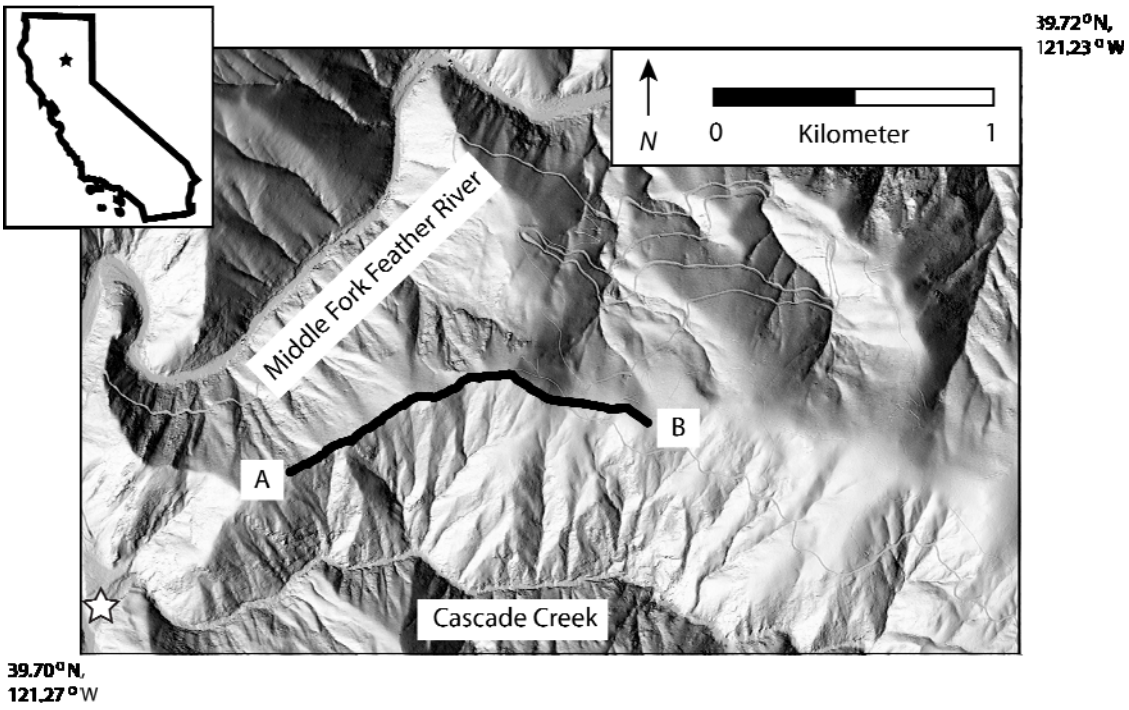

Figure 1. Site map. (Inset) Map of California with star indicating field site. (Main) Hillshade of Cascade Ridge with transect delineated by the black line. The Middle Fork of the Feather River is to the north of the ridge and Cascade Creek is to the south. The Feather River, truncated by the left boundary of the image, flows from NE to SW and forms a tributary junction with Cascade Creek (shown with the white star) and serves as its baselevel. The 'A' and 'B' indicate the ends of the transect and are referred to in later figures.

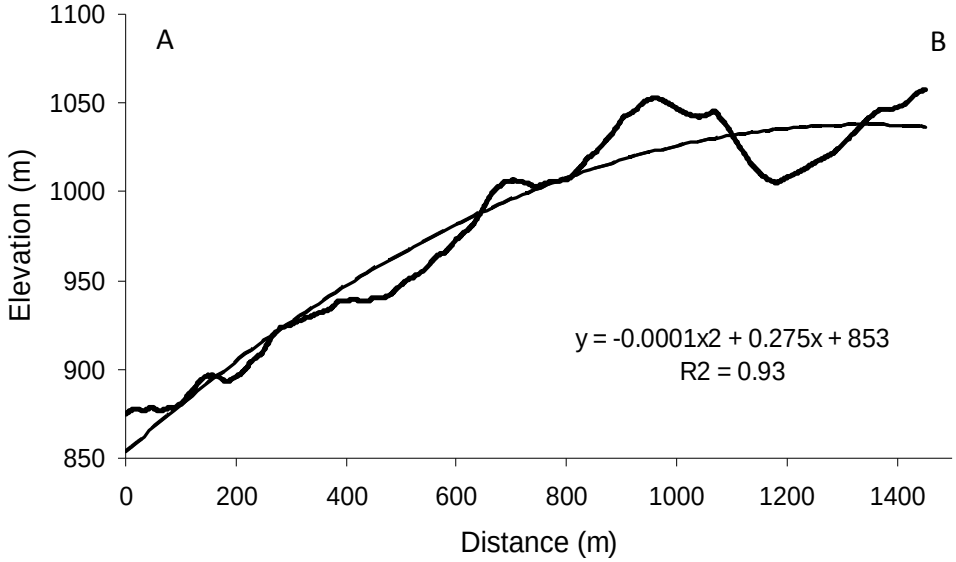

Figure 2. Second-order polynomial fit to ridgeline elevations along study reach. Ridgeline elevations were subtracted from the polynomial to isolate the local topography. 'A' and 'B' refer to transect ends shown in Figure 1.

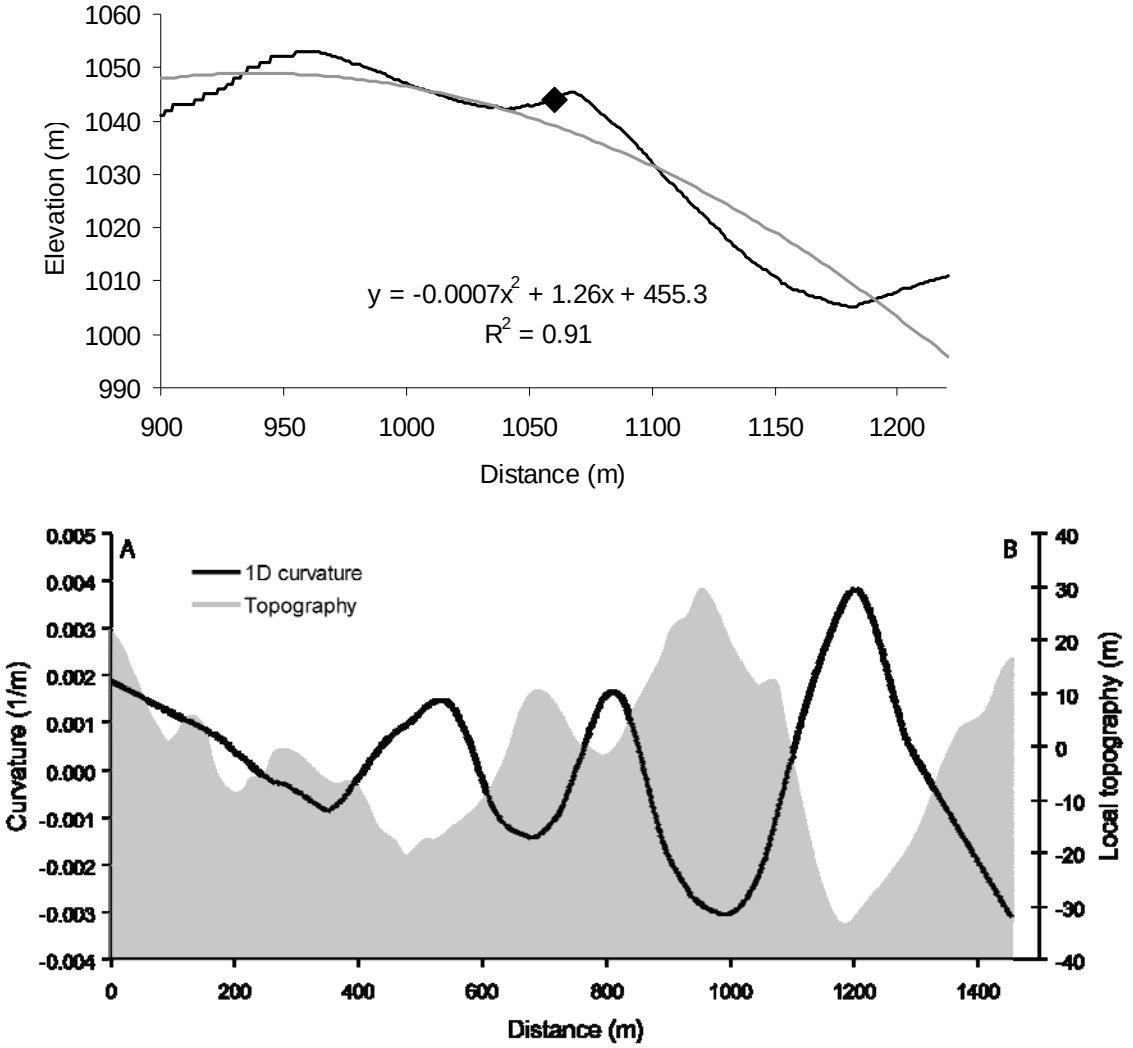

Figure 3. (A) Example of a ridgeline section fitted with a 2nd-order polynomial over a 320-m sliding window. The topographic curvature at the midpoint of this section, designated with the diamond, is the 2nd derivative of the polynomial function, -0.0014. (B) 1D curvature along ridgeline derived from 2nd-order polynomial. Local topography shown here to emphasize correspondence between curvature values and topography. High positive curvatures are at the saddles and low negative curvatures are at the knobs.

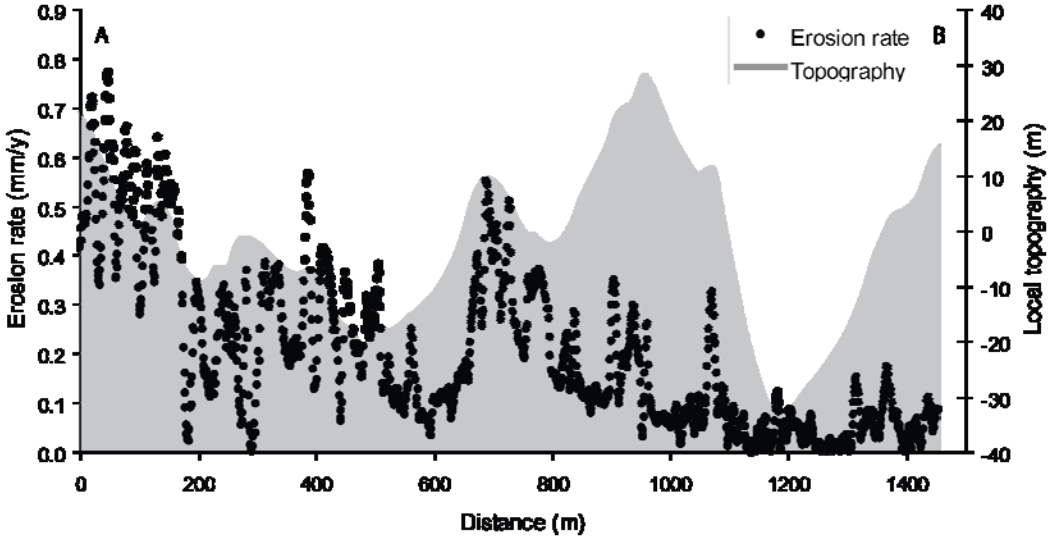

Figure 4. Erosion rate calculated from 2D curvature compared to the local ridgeline topography. The erosion rate calculation appears to be influenced by the local topography whereby the knobs have higher erosion rates than the saddles.

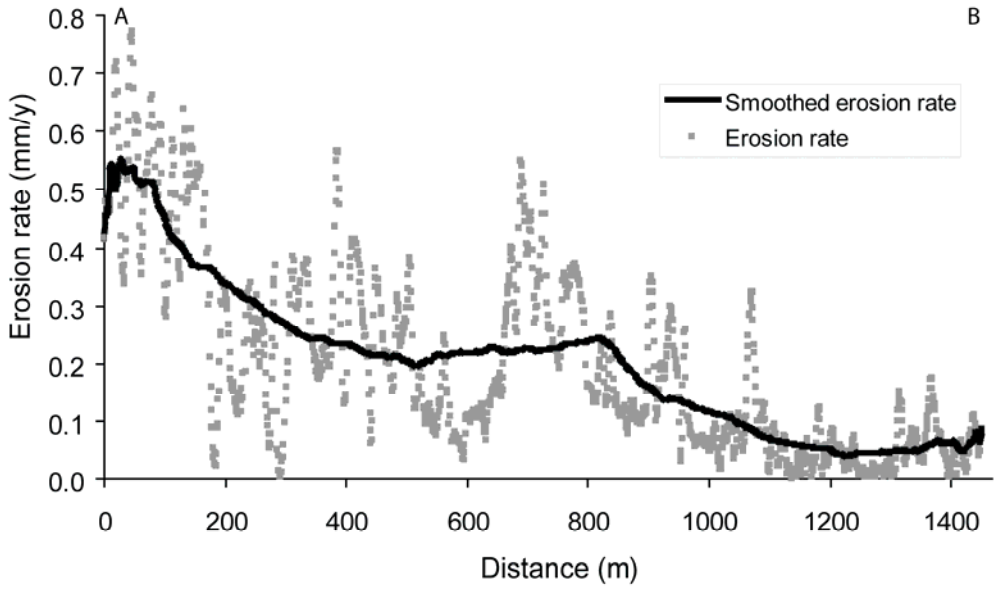

Figure 5. Erosion rate calculated from 2D ridgeline curvature averaged over a 320-m window to reduce the effects of the local topography. There appear to be 3 different erosional regimes along the transect: ~0.52 mm/y along the proximal portion, ~0.22 mm/y in the middle, and ~0.06 mm/y along the distal section. The transition between each section is not sharp, likely a consequence of a gradual geomorphic adjustment to the advance of the incision wave(s).

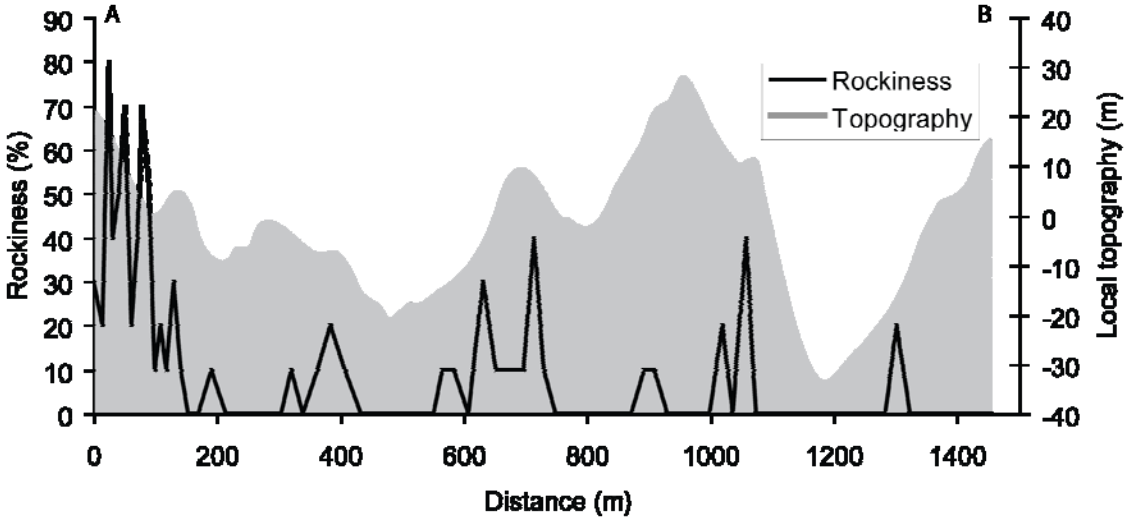

Figure 6. Comparison of surface material and local topography. The rapidly eroding end of the transect (0 – 200 m) has a substantially greater amount of large clasts and bedrock at the surface than the slowly eroding portions. Knobs and steep sideslopes tend to be more rocky although the relationship between rockiness and topography is not strong.

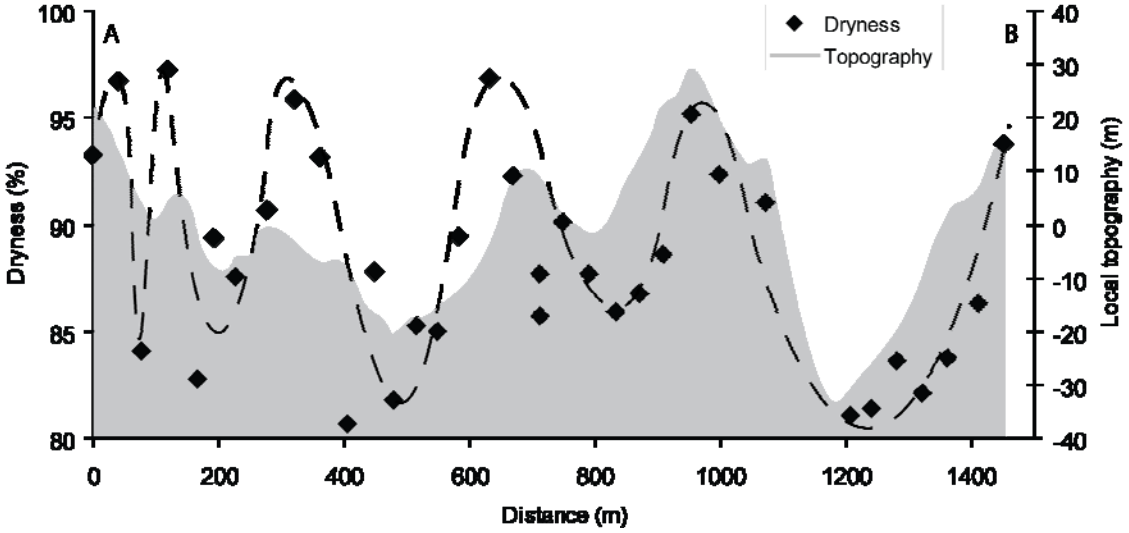

Figure 7. Soil dryness (i.e., 100 - % moisture) and local topography along the ridge. The driest regolith is associated with knobs and southwest-facing sideslopes. Wettest regoliths in the saddles. Dashed line fit by eye to emphasize trends in regolith moisture. Regolith moisture represented by 'dryness' to facilitate comparison with the local topography.

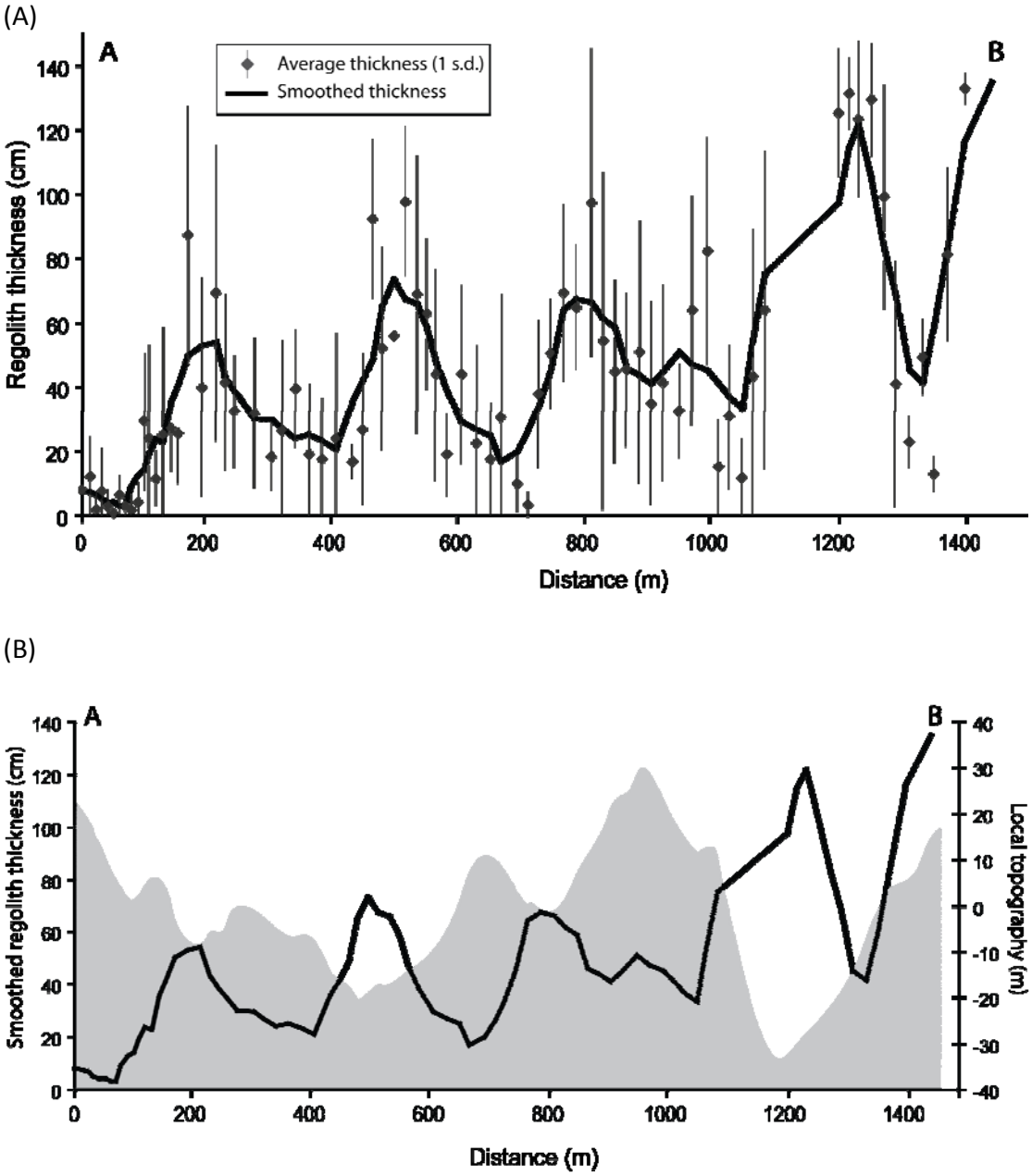

Figure 8. (A) Regolith thickness along the transect. A 5-pt moving average of thickness reveals a sinusoidal pattern along the ridge. (B) Regolith thickness (moving average) and local topography are nearly mirror images of each other. The regolith is thickest in the saddles and thinnest on the knobs. Note the general increase in regolith thickness towards the distal end of the transect where the erosion rates are lower.

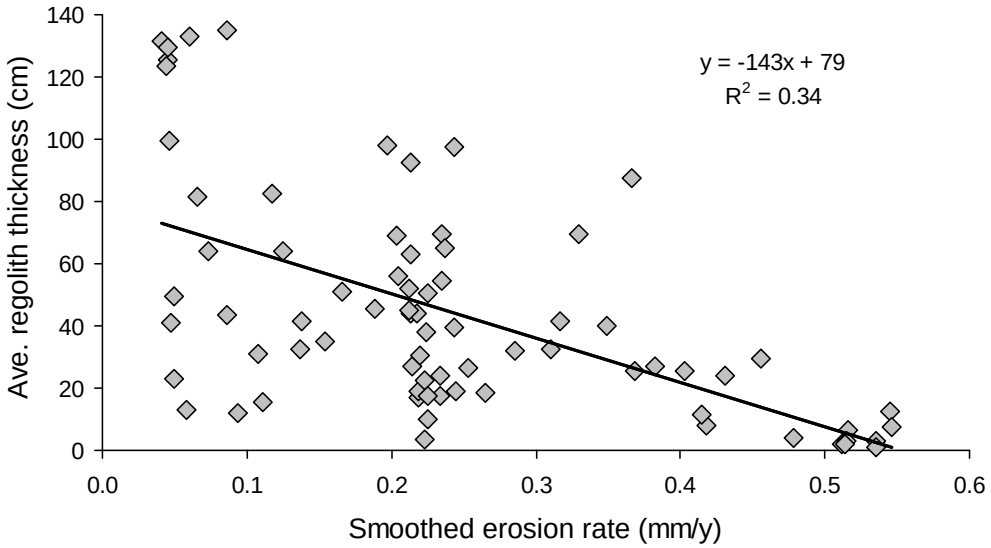

Figure 9. Regolith thickness vs. calculated erosion rate. The erosion rate used here is the smoothed rate shown in Figure 5. Because regolith thickness exceeded the reach of the probe in the slowly eroding portion of the ridge, the data points in the upper left of the plot under-represent the true thickness and, as a result, the slope of the regression should be steeper.

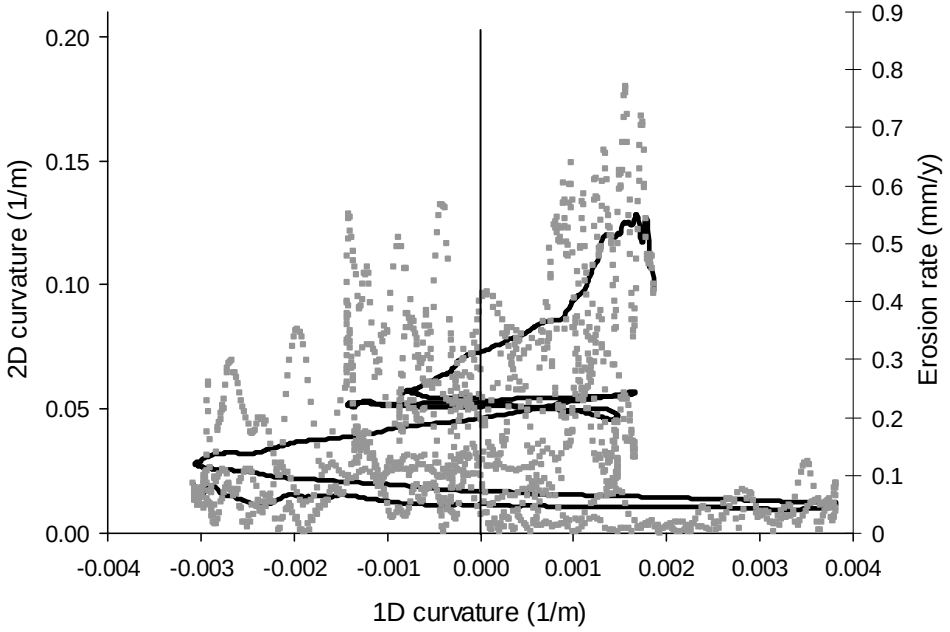

Figure 10. Plot of 2D curvature and erosion rate vs. 1D ridgeline curvature. Although the erosion rate was calculated from the 2D curvature, it is uncorrelated with the 1D curvature. The spatial autocorrelation in the raw data is due to the sliding-window technique of calculating the 1D curvature. The 'smoothed erosion rate' was determined by averaging over a 320-m sliding window to damp the effects of local topography on the calculation of erosion rate (see Figure 5). The three erosional regimes create the three plateaus seen in the line plot.

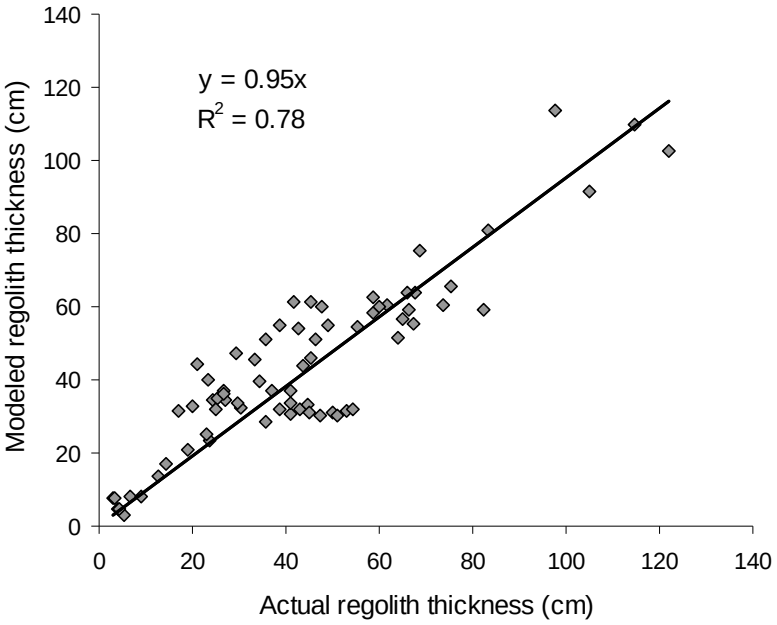

Figure 11. Regolith thickness modeled from the 1D ridgeline curvature and the calculated erosion rate. Measured regolith thickness values were smoothed with a 5-pt moving window to damp meter-scale variations not captured in our study. The similarity between the modeled and actual regolith thicknesses suggest that 1D curvature and erosion rate are the primary factors in controlling regolith thickness along Cascade Ridge at the 10^2-m scale. The constant in the regression indicates that regolith thickness is consistently underpredicted, albeit by a small amount.

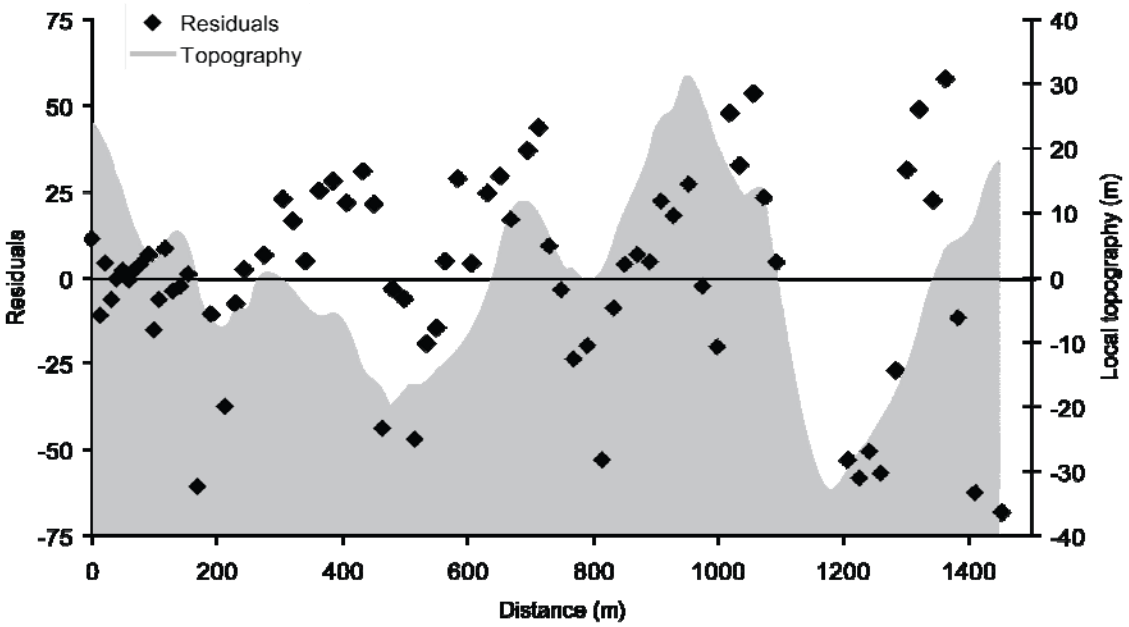

Figure 12. Residuals from the regolith thickness regression equation compared to the local topography. The non-random distribution of the residuals indicates that the 1D ridgeline curvature is not fully capturing the effects of the local topography.

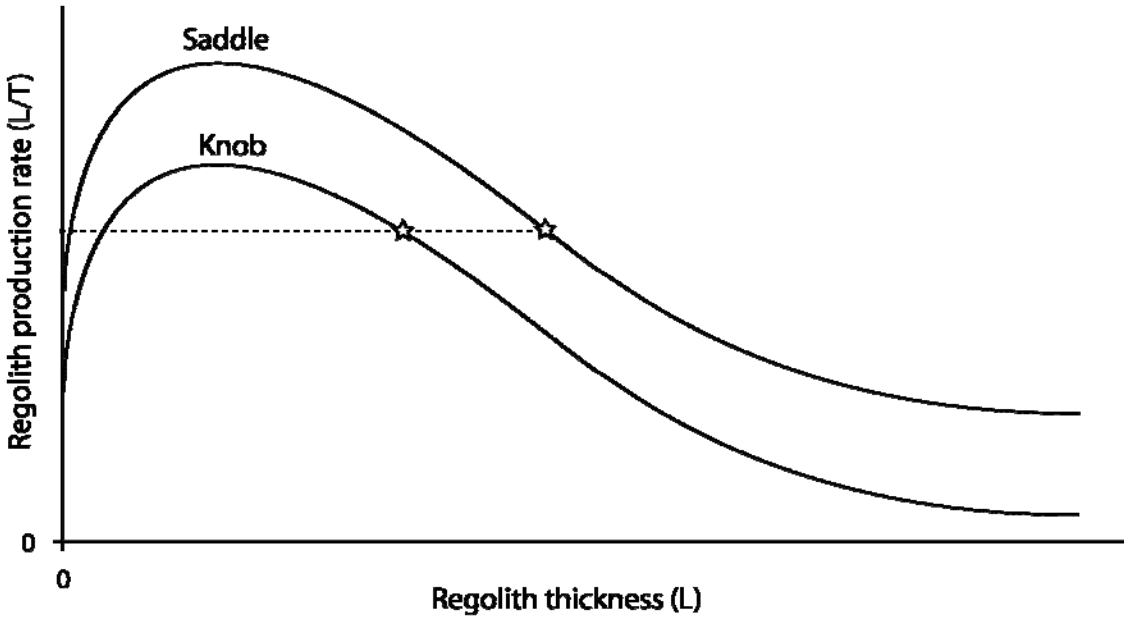

Figure 13. Different soil production functions depending on topographic position. Although knobs and saddles may be eroding at the same rate, they may host different steady-state regolith thicknesses because of different local conditions (indicated by stars). For example, saddles may have higher rates of regolith production for a given regolith thickness because they remain wetter for longer periods of time.

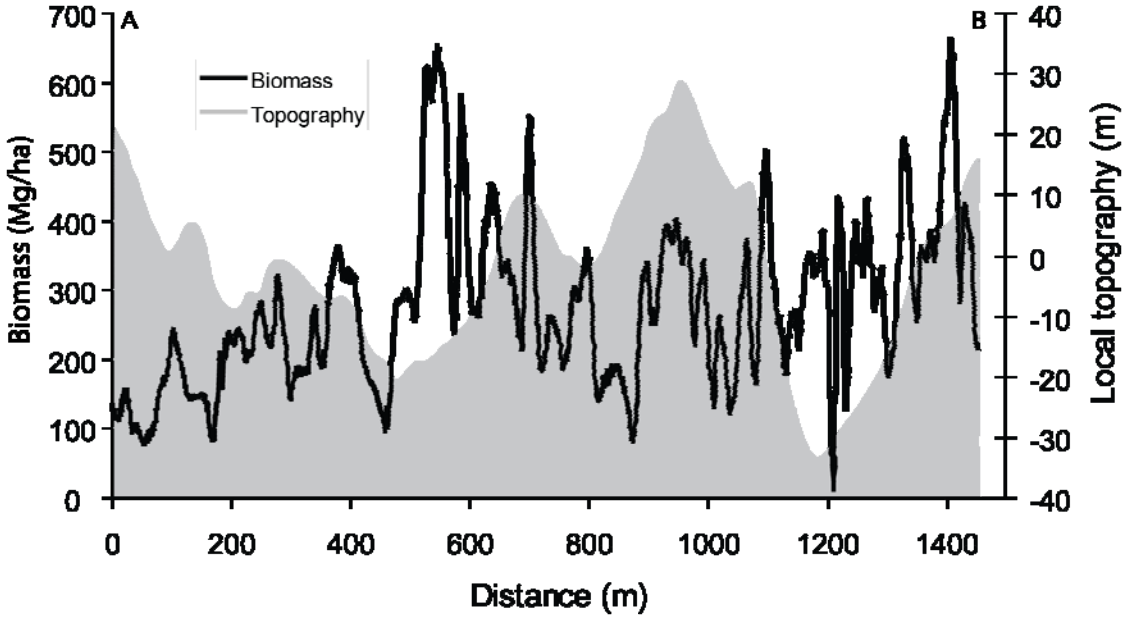

Figure 14. Aboveground biomass and local topography along the ridge. Biomass increases nearly 4-fold from the rapidly eroding portion of the ridge to the slowly eroding portion. Biomass determined with mean canopy heights derived from LiDAR data (Milodowski *et al.*, 2015).

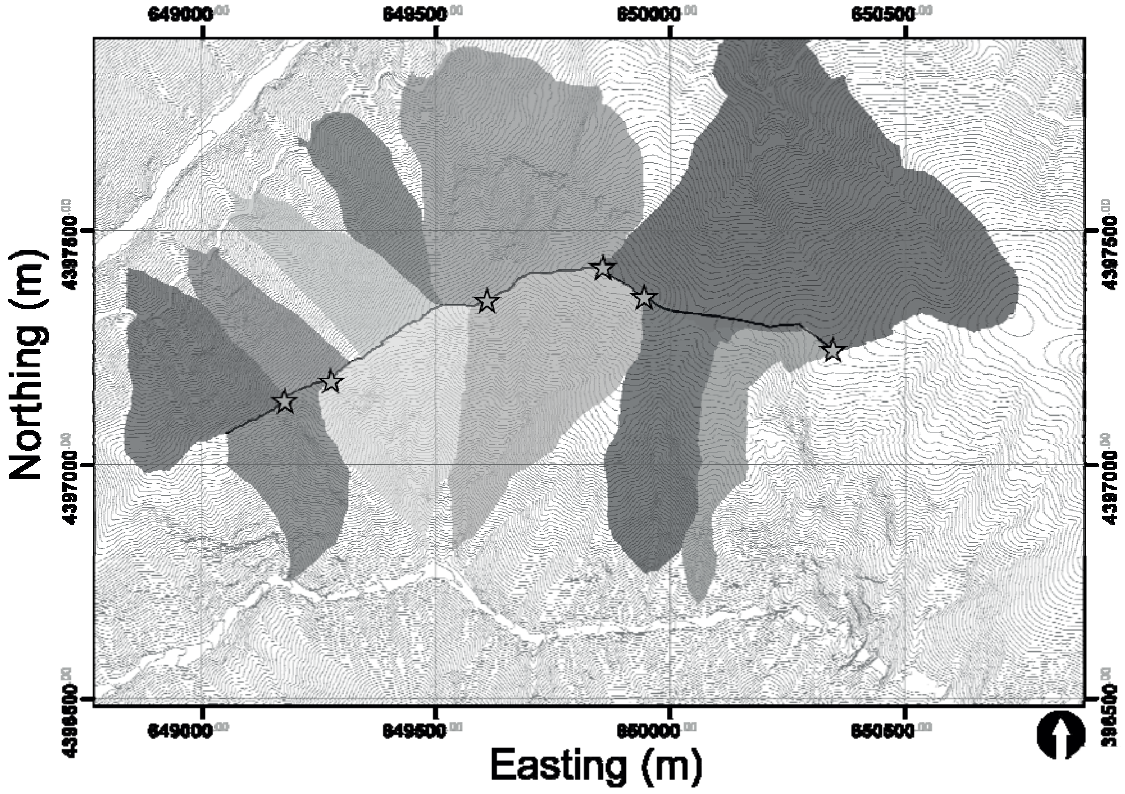

Figure 15: Knobs (stars) and basins along Cascade Ridge. The knobs along Cascade Ridge are often the uppermost extent of spur ridges bounding the basins that drain from the ridge to the valley bottom (shaded).